Systematic studies of hexanuclear {MIII4LnIII2} complexes (M = Fe, Ga; Ln = Er, Ho): structures, magnetic properties and SMM behavior

Article (Accepted Version)

Systematic Studies of Hexanuclear $\{M^{III}_4Ln^{III}_2\}$ Complexes (M = Fe, Ga; Ln = Er, Ho): Structures, Magnetic Properties and SMM Behavior

Sihuai Chen,[a,b] Valeriu Mereacre,*[a] George Kostakis,[c] Christopher E. Anson[a] and Annie K. Powell*[a,d]

Four isostructural $M^{III}_4Ln^{III}_2$ coordination clusters, $[M_4Ln_2(\mu_3\text{-}OH)_2(n\text{bdea})_4(C_6H_5COO)_8]\cdot$MeCN (M = Fe, Ln = Er (**1**); M = Ga, Ln = Er (**2**); M = Fe, Ln = Ho (**3**); M = Ga, Ln = Ho (**4**)) have been synthesized and characterized. Single-crystal X-ray diffraction and X-ray powder diffraction studies revealed that all four compounds crystallize isomorphously to each other, and to the previously reported $M^{III}_4Dy^{III}_2$ (M = Fe or Ga) and $Fe^{III}_4Y^{III}_2$ analogues. DC magnetic susceptibility measurements for compounds **1**-**4**, taken in combination with those for the $Fe^{III}_4Y^{III}_2$ analogue, indicated that the interactions between Er^{III} ions are weakly ferromagnetic and the Fe^{III}-Er^{III} interactions are very weakly antiferromagnetic, while the Ho^{III}-Ho^{III} and Fe^{III}-Ho^{III} interactions are both negligible. By comparison, for the $Fe^{III}_4Dy^{III}_2$ analogue, the Dy^{III}-Dy^{III} interactions are antiferromagnetic while the Fe^{III}-Dy^{III} are ferromagnetic. Both Er analogues **1** and **2** display single-molecule magnet (SMM) behavior with the effective energy barrier U_{eff} increasing from 12.8 K (for Fe_4Er_2 **1**) to 53.5 K (for Ga_4Er_2 **2**), indicating that the very weak 3d-4f interaction enhances the QTM effect.

Introduction

Single-molecule magnets (SMMs) are a class of molecular metal clusters, which display slow relaxation of the magnetization at low temperature.[1] The combination of a high spin ground state and a large uniaxial magnetoanisotropy leads to higher relaxation energy barrier U_{eff} and blocking temperature T_B for SMMs. Due to the large unquenched orbital angular momentum, Ln^{III} ions can exhibit large single-ion magnetic anisotropies, leading to significant energy barriers in lanthanide-based SMMs.[2-4] Therefore, the synthesis and characterization of high-nuclearity 3d-4f SMMs have attracted intensive attention in recent years. [5-9] Although many studies on 4f-4f or 3d-3d interactions have been reported,[10-17] research on 3d-4f exchange interactions is less developed.[18-24]

Furthermore, according to the model of free-ion electron densities for all Ln^{III} ions, the shape of the 4f electron density for the Dy^{III} ion is oblate, while that for Er^{III} is prolate.[25] Therefore, in order to maximize the magnetic anisotropy, a sandwich-type ligand geometry with harder or negatively-charged ligand atoms predominantly in axial positions is expected to be appropriate for Dy^{III}, while a ligand field with such harder atoms mainly in an equatorial coordination positions should be necessary for Er^{III}.[26-32] However, 3d-Er^{III} coordination clusters showing SMM behavior are rare in comparison to 3d-Dy^{III} or 3d-Tb^{III} clusters.[17,18,33] Sessoli et al. recently published two isostructural Ln(trensal) complexes with identical ground state J = 15/2, namely the easy-plane Dy(trensal) and easy-axis Er(trensal).[34] Perhaps surprisingly, both of these show slow magnetic relaxation at low temperature, indicating the complexity of the relationship between the magnetoanisotropy and the dynamic of magnetic relaxation at low temperature in lanthanide-based SMMs.

Recently, we reported a series of heterometallic complexes $[M_4Ln_2(\mu_3\text{-}OH)_2(n\text{bdea})_4(C_6H_5COO)_8]\cdot$MeCN (M = Fe, Ln = Dy; M = Ga, Ln = Dy; M = Fe, Ln = Y) which enabled us to separate out the magnetic contributions of the Fe^{III} and Dy^{III} ions and the Fe^{III}-Fe^{III}, Dy^{III}-Dy^{III} and Fe^{III}-Dy^{III} interactions within the systems.[35,36] To investigate further the Fe^{III}-Ln^{III} and Ln^{III}-Ln^{III} interactions and the relaxation of the magnetization in such $M^{III}_4Ln^{III}_2$ systems, we have now extended that work from Dy^{III} to Ho^{III} and Er^{III}, synthesising the isostructural Ho and Er analogues of the Dy compounds, $[M^{III}_4Ln^{III}_2(\mu_3\text{-}OH)_2(n\text{bdea})_4(C_6H_5COO)_8]\cdot$MeCN (M = Fe, Ln = Er (**1**); M = Ga, Ln = Er (**2**); M = Fe, Ln = Ho (**3**); M = Ga, Ln = Ho (**4**)). We here describe the syntheses, structures and magnetic properties of these four compounds. Comparison of these results with data from the previously reported Fe_4Y_2 and M_4Dy_2 compounds shows that trends in Fe-Ln and Ln-Ln interactions are not simple. Compounds **1** and **2** show slow relaxation of their magnetisation, with **1** another example of a 3d-Er^{III} SMM; replacement of paramagnetic Fe^{III} in **1** by diamagnetic Ga^{III} in **2** significantly improves the SMM properties.

Experimental

Synthesis. Unless otherwise stated, all chemicals and solvents were obtained from commercial sources and were used without further purification. All reactions were carried out under aerobic conditions. $[Fe_3O(C_6H_5CO_2)_6(H_2O)_3]\cdot(O_2CC_6H_5)$ and $[Ga_3O(C_6H_5CO_2)_6(H_2O)_3]\cdot(O_2CC_6H_5)\cdot2H_2O$ were prepared according to the literature procedure.[37,38] Elemental analyses for C, H, N were performed using an Elementar Vario EL analyzer and were carried out at the Institute of Inorganic Chemistry, Karlsruhe Institute of Technology. IR spectra were measured on a Perkin-Elmer Spectrum One spectrometer using KBr pellets and the X-ray powder diffraction patterns were measured at room temperature using a Stoe STADI-P diffractometer with a Cu-Kα radiation.

Synthesis of $[Fe_4Er_2(\mu_3\text{-}OH)_2(n\text{bdea})_4(C_6H_5COO)_8]\cdot$MeCN (1)

A solution of $[Fe_3O(C_6H_5COO)_6(H_2O)_3]\cdot(C_6H_5COO)$ (0.127 g, 0.12 mmol), $Er(NO_3)_3\cdot6H_2O$ (0.056 g, 0.12 mmol) and $n$bdeaH$_2$ (0.161 g, 1.00 mmol) in MeCN (10 ml) was stirred at room temperature for one hour. The resulting solution was left undisturbed in air. Yellow blocks were crystallized after three hours, washed with MeCN and dried in the air. Yield: 47% (based on Er). Anal. Calc. for $C_{90}H_{113}N_5O_{26}Fe_4Er_2$: C, 48.28; H, 5.09; N, 3.13; found C, 48.36; H, 4.87; N, 3.03%. IR (KBr)/cm^{-1}: 3450 (br), 2958 (s), 1965 (w), 1643 (s), 1599 (s), 1558 (s), 1492 (m), 1449 (s), 1400 (vs),

1323 (s), 1301 (s), 1175 (m), 1135 (m), 1085 (s), 1026 (s), 908 (m), 825 (m), 721 (s), 691 (m), 678 (s), 632 (w), 590 (m), 538 (mw).

Synthesis of $[Ga_4Er_2(\mu_3\text{-}OH)_2(n\text{bdea})_4(C_6H_5COO)_8]\cdot$MeCN (2)

The synthetic method for **2** was similar to that of **1** but replacing $[Fe_3O(C_6H_5COO)_6(H_2O)_3]\cdot(C_6H_5COO)$ with $[Ga_3O(C_6H_5CO_2)_6(H_2O)_3]\cdot(O_2CC_6H_5)\cdot 2H_2O$. Colorless crystals were obtained after one day, washed with MeCN and dried in the air. Yield: 55% (based on Er). Anal. Calc. for $C_{90}H_{113}N_5O_{26}Ga_4Er_2$: C, 47.12; H, 4.96; N, 3.05; found C, 47.01; H, 5.08; N, 2.99%. IR (KBr)/cm^{-1}: 3433 (br), 2960 (s), 1962 (w), 1643 (s), 1598 (s), 1558 (s), 1493 (m), 1449 (s), 1401 (vs), 1323 (s), 1301 (s), 1174 (m), 1135 (m), 1085 (s), 1026 (s), 905 (m), 823 (m), 721 (s), 691 (m), 678 (s), 632 (w), 590 (m), 538 (mw).

Synthesis of $[Fe_4Ho_2(\mu_3\text{-}OH)_2(n\text{bdea})_4(C_6H_5COO)_8]\cdot$MeCN (3)

The synthetic method for **3** was similar to that of **1** but replacing $Er(NO_3)_3\cdot 6H_2O$ with $Ho(NO_3)_3\cdot 6H_2O$. Yellow crystals were obtained after one day, washed with MeCN and dried in the air. Yield: 59% (base on Ho). Anal. Calc. for $C_{90}H_{113}N_5O_{26}Fe_4Ho_2$: C, 48.38; H, 5.10; N, 3.13; found C, 48.17; H, 5.01; N, 3.05%. IR (KBr)/cm^{-1}: 3437 (br), 2959 (s), 1962 (w), 1643 (s), 1598 (s), 1558 (s), 1493 (m), 1449 (s), 1399 (vs), 1322 (s), 1301 (s), 1174 (m), 1135 (m), 1084 (s), 1026 (s), 908 (m), 824 (m), 721 (s), 690 (m), 677 (s), 632 (w), 590 (m), 537 (mw).

Synthesis of $[Ga_4Ho_2(\mu_3\text{-}OH)_2(n\text{bdea})_4(C_6H_5COO)_8]\cdot$MeCN (4)

The synthetic method for **4** was similar to that of **3** but replacing $[Fe_3O(C_6H_5COO)_6(H_2O)_3]\cdot(C_6H_5COO)$ with $[Ga_3O(C_6H_5CO_2)_6(H_2O)_3]\cdot(O_2CC_6H_5)\cdot 2H_2O$. Colorless crystals were obtained after one day, washed with MeCN and dried in the air. Yield: 38% (base on Ho). Anal. Calc. for $C_{90}H_{113}N_5O_{26}Ga_4Ho_2$: C, 47.21; H, 4.97; N, 3.06; found C, 47.07; H, 4.85; N, 2.98%. IR (KBr), /cm^{-1}: 3445 (br), 2960 (s), 1960 (w), 1643 (s), 1599 (s), 1559 (s), 1492 (m), 1450 (s), 1400 (vs), 1322 (s), 1300 (s), 1175 (m), 1135 (m), 1085 (s), 1027 (s), 909 (m), 823 (m), 721 (s), 690 (m), 678 (s), 632 (w), 589 (m), 538 (mw).

Magnetic Measurements. The magnetic susceptibility measurements were carried out using a Quantum Design SQUID magnetometer MPMS-XL. This magnetometer works between 1.8 and 300 K for dc applied fields ranging from -7 to 7 T. Measurements were carried out on finely ground polycrystalline samples. AC susceptibility measurements were measured with an oscillating ac field of 3 Oe and ac frequencies ranging from 1 to 1500 Hz. The magnetic data were corrected for the sample holder.

X-ray Crystallography. Data were collected on Rigaku Oxford Diffraction Supernova E (**2**) or Stoe IPDS (**3**) diffractometer susing graphite-monochromated Mo-Kα radiation, and were corrected for absorption. Structures were solved using dual-space direct methods (SHELXT),[39] followed by full-matrix least-squares refinement against F^2 (all data) using SHELXL-2014.[40] Anisotropic refinement was used for all ordered non-hydrogen atoms; disorder within the nbdea ligands was modelled using partial occupancy isotropic carbon atoms with geometrical similarity restraints. O-H hydrogen atoms in **2** were refined, whereas all other H-atoms were placed in calculated positions. The crystallographic and structure refinement data for all compounds are summarised in Table 1. Crystallographic data (excluding structure factors) for the fully refined structures in this paper have been deposited with the Cambridge Crystallographic Data Centre as supplementary publication nos. CCDC 1505110 and 1505111. Copies of the data can be obtained from https://summary.ccdc.cam.ac.uk/structure-summary-form

Results and discussion

Synthesis and Crystal Structures. The reaction of $Ln(NO_3)_3\cdot 6H_2O$ (Ln = Er, Ho) and $[M_3O(O_2CC_6H_5)_6(H_2O)_3]\cdot(O_2CC_6H_5)$ (M = Fe, Ga) with $n$bdeaH$_2$ in MeCN at room temperature produced the compounds $[M^{III}_4Ln^{III}_2(\mu_3\text{-}OH)_2(n\text{bdea})_4(C_6H_5COO)_8]\cdot$MeCN (M = Fe, Ln = Er (**1**); M = Ga, Ln = Er (**2**); M = Fe, Ln = Ho (**3**); M = Ga, Ln = Ho (**4**)). The structures of compound **2** and **3** were determined by single-crystal X-ray diffraction studies; both compounds crystallize in the monoclinic space group $P2_1/c$ with Z = 4, with the cluster molecules occupying general positions. Comparison with the unit cells of **1** and **4** showed that all four of the compounds reported here crystallised isotypically to each other and to the previously reported Fe_4Dy_2, Fe_4Y_2 and Ga_4Dy_2 analogues.[35,36]

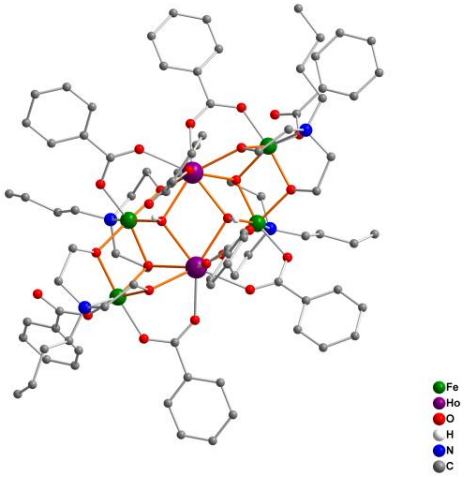

Fig. 1 The $[Fe_4Ho_2(\mu_3\text{-}OH)_2(n\text{bdea})_4(C_6H_5COO)_8]$ cluster in **3**. Organic H-atoms and lattice MeCN omitted for clarity.

Table 1 Crystallographic and structure refinement data for **1**-**4**.

	1	**2**	**3**	**4**
Formula	$C_{90}H_{113}N_5O_{26}Fe_4Er_2$	$C_{90}H_{113}N_5O_{26}Ga_4Er_2$	$C_{90}H_{113}N_5O_{26}Fe_4Ho_2$	$C_{90}H_{113}N_5O_{26}Ga_4Ho_2$
M_r	2238.81	2294.25	2234.11	2289.66
Crystal system	monoclinic	monoclinic	monoclinic	monoclinic
Space group	$P2_1/c$	$P2_1/c$	$P2_1/c$	$P2_1/c$
T (K)	298	150(2)	243(2)	298
a (Å)	15.22	15.0782(4)	15.221(4)	15.23
b (Å)	29.03	29.1333(6)	29.282(5)	29.31
c (Å)	22.35	22.2449(7)	22.420(5)	22.49
α (°)	90	90	90	90
β (°)	108.15	106.817(3)	108.00(3)	107.39
γ (°)	90	90	90	90
V (Å^3)	9383	9353.8(5)	9504(4)	9581
Z	4	4	4	4
D_{calc} (g cm^{-3})		1.629	1.561	
F (000)		4624	4536	
μ (mm^{-1})		2.987	2.315	
Reflections collected		47861	58808	
Unique reflections		21481	16957	

R_{int}	0.0284	0.0611
Parameters	1146	1141
R_1 ($I > 2\sigma(I)$)	0.0318	0.0441
wR_2 (all data)	0.0673	0.1153
S (all data)	1.037	0.953
Largest peak/hole (e/Å^3)	+0.97 / -0.99	+1.27 / -1.51
CCDC	1505110	1505111

The structure of the Fe_4Ho_2 compound **3** is shown in Fig. 1. The hexanuclear core is made up of a central $Ho_2(\mu_3\text{-}OH)_2$ core, which is flanked by two $Fe_2(n\text{bdea})_2$ moieties. Within each of the latter, each Fe^{III} centre is chelated by a doubly-deprotonated $(n\text{bdea})^{2-}$ ligand, with one oxygen from each of these ligands bridging to the other Fe^{III} in the dinuclear unit. One of these two bridging oxygens also coordinates to a Ho^{III} forming a μ_3-alkoxo bridge. The remaining deprotonated oxygen from each diethanolamine ligand then bridges between its respective Fe^{III} and a Ho^{III}, completing the core structure. Peripheral ligation is then provided by four *syn,syn*-bridgingand four unidentate benzoates. Overall the molecule has idealised C_2 symmetry (in Figure 1 the twofold axis is normal to the plane of the paper and midway between the two Ho centres) with both Fe_2 units displaced to the same side of the $Ho_2(\mu_3\text{-}OH)_2$ plane. Both Ho^{III} ions are eight-coordinated with square antiprismatic geometry, while all the Fe^{III} ions are hexacoordinate with distorted octahedral geometries.

Magnetic Properties. The dc magnetic susceptibilities of **1-4** were measured under an applied magnetic field of 1000 Oe over the temperature range 1.8 - 300 K. As shown in Fig. 2a, the χT value for compound **1** at 300 K is 36.2 cm^3 K mol^{-1}, lower than the expected value of 40.5 cm^3 K mol^{-1} for four Fe^{III} (S = 5/2, g = 2) and two Er^{III} (S = 3/2, L = 6, $^4I_{15/2}$, g = 6/5) non-interacting ions. On lowering the temperature, the χT value decreases continuously, reaching 19.2 cm^3 K mol^{-1} at 5 K. This decrease results from a combination of thermal depopulation of excited M_J sub-levels of the Er^{III} cations and antiferromagnetic Fe^{III}-Fe^{III} interactions, with J_{FeFe} found to be -7 cm^{-1} in the isostructural $Fe^{III}_4Y^{III}_2$ analogue **5**.[35] Below 5 K, χT then increases slightly to reach 20.1 cm^3 K mol^{-1} at 2 K, with this upturn due to the presence of weak ferromagnetic interactions, either Er^{III}-Er^{III} and/or Fe^{III}-Er^{III}, in **1**. Comparison of the data for **1** with those for **2** and **5** now enable us to identify the source of these ferromagnetic interactions.

For compound **2**, containing diamagnetic Ga^{III} ions in place of Fe^{III}, the χT value of 23.2 cm^3 K mol^{-1} at 300 K is in good agreement with the expected value of 23.0 cm^3 K mol^{-1} for two isolated Er^{III} (S = 3/2, L = 6, $^4I_{15/2}$, g = 6/5) ions. On lowering temperature from 300 K to 100 K, the χT product for **2** remains almost constant, and then drops slightly and steadily to 19.4 cm^3 K mol^{-1} at 12 K, followed by an increase to reach 21.1 cm^3 K mol^{-1} at 2 K (Fig. 2a). Figure 2a also shows the corresponding curve for the Fe_4Y_2 analogue **5**,[35] together with a plot of the sum of the curves for **2** and **5** (Ga_4Er_2 + Fe_4Y_2), with an enlargement of the 2-50 K regions of the Fe_4Er_2 and (Ga_4Er_2 + Fe_4Y_2) curves shown in Figure 3.

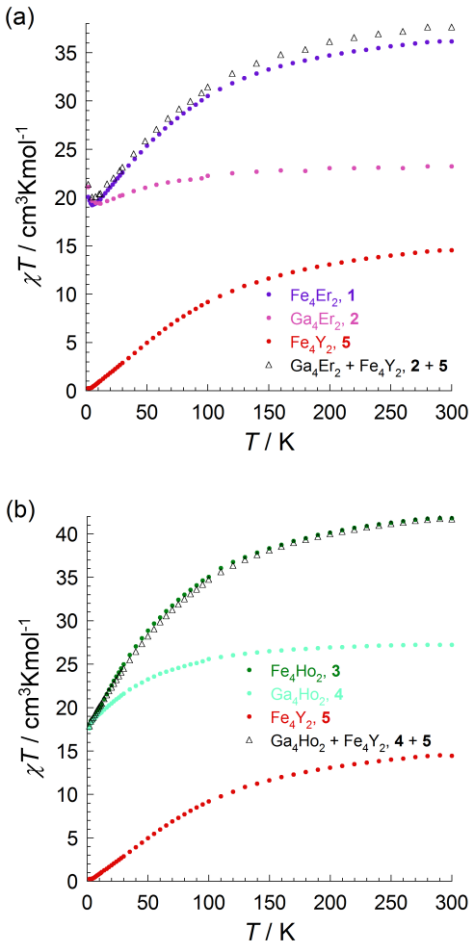

Fig. 2 (above) Temperature dependence of the χT product for compounds **1**, **2** and **5** with a plot of the sum of the χT values for **2** and **5**; (below) the corresponding plots for **3**, **4** and **5** with the plot of the sum of the χT values for **4** and **5**. (Data for **5** from Ref. 35).

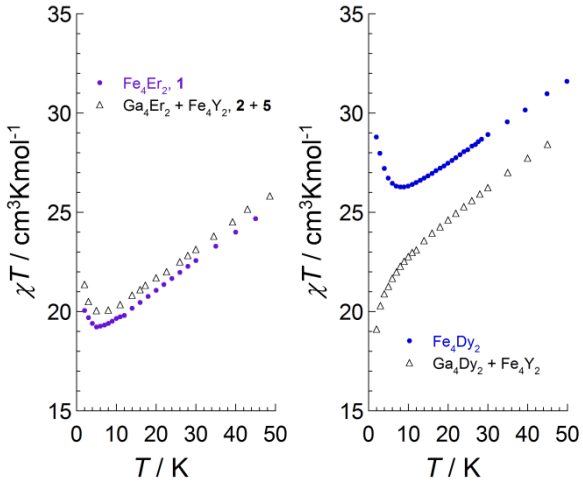

Fig. 3 (left) χT -v- T plot below 50 K for **1** (Fe_4Er_2) compared with a plot of the sum of the χT values for **2** (Ga_4Er_2) and **5** (Fe_4Y_2); (right) χT -vs- T plot below 50 K for the previously reported **6** (Fe_4Dy_2) compared with a plot of the sum of the χT values for **7**

(Ga_4Dy_2) and **5** (Fe_4Y_2). (Data for **5** and **6** from Ref. 35, data for **7** from Ref. 36).

The increase of the χT product for **2** at low temperature indicates that the magnetic interaction between the two central Er^{III} ions is ferromagnetic, since these are the only magnetic ions in the molecule. Furthermore, the Fe^{III}-Er^{III} exchange interactions in **1** can be estimated by comparing the temperature dependence of the sum of the χT values for Ga_4Er_2 (**2**) and Fe_4Y_2 (**5**) (which between them contain the contributions from the Er^{III}-Er^{III} and Fe^{III}-Fe^{III} interactions together with the thermal depopulation of Er^{III} M_J sub-levels) with that of χT for Fe_4Er_2 (**1**) (which contains all these contributions, but additionally the Fe^{III}-Er^{III} interactions). As can be seen in Figures 2 and 3, the χT *vs* T curves for **1** and for {**2** + **5**} are very similar, with the non-superposition resulting from only a slight scaling issue. Importantly, both curves show essentially identical upturns at temperatures below 10 K, indicating that the Fe^{III}-Er^{III} interactions are here negligible or very weak antiferromagnetic.

The χT value for compound **3** at 300 K is 41.8 cm^3 K mol^{-1}, which is lower than the value of 45.6 cm^3 K mol^{-1} expected for isolated four Fe^{III} (S = 5/2, g = 2) and two Ho^{III} (S = 2, L = 6, $^5I_8$, g = 5/4) spin centers. For **4**, the χT product of 27.2 cm^3 K mol^{-1} is in relatively good agreement with the expected value of 28.1 cm^3 K mol^{-1} for two magnetically uncoupled Ho^{III} (S = 2, L = 6, $^5I_8$, g = 5/4) ions. The χT products for both **3** and **4** decrease steadily with decreasing temperature down to 1.8 K (Fig. 3). The curves for Fe_4Ho_2 (**3**) and for {Ga_2Ho_2 (**4**) + Fe_4Y_2 (**5**)} (Figure 2) are almost exactly superposed. Both curves show the same almost linear decrease below 30 K, with neither upturn nor downturn at the lowest temperatures. It can be concluded that for the Ho^{III} compounds, the Ho^{III}-Ho^{III} and Fe^{III}-Ho^{III} interactions are all negligible.

Our earlier data for the Ga_4Dy_2 (**6**)[36] and Fe_4Dy_2 (**7**)[35] analogues can be used to construct a similar pair of χT -v- T curves (Figure 3) for an instructive visual comparison to those for Er^{III}. The curves for **6** and {**5** + **6**} show a steepening of the decrease in χT below about 8 K, which was interpreted as the effect of antiferromagnetic Dy^{III}-Dy^{III} interactions superimposed on the thermal depopulation of Dy^{III} M_J sub-levels.[29] The curve for Fe_4Dy_2 (**7**), by contrast shows a significant upturn below 10 K, which is significantly larger than those seen for the Er^{III} analogues. Such an upturn indicates that the Fe^{III}-Dy^{III} interactions in **7** have forced the two Dy^{III} spins into a coparallel ferromagnetic arrangement. Note that this does not necessarily imply that these interactions are themselves ferromagnetic. If one only considers the Fe-Dy interactions within the central Fe_2Dy_2 butterfly, then either ferro- or antiferromagnetic Fe-Dy interactions would force the Dy spins coparallel, provided they were all similar and significantly stronger than the Dy-Dy.

The field dependence of magnetization at low temperature for compounds **1**-**4** is shown in Fig. S1 and S2. The lack of saturation even up to 70 kOe suggests the thermally and/or field-induced population of low lying excited states, but also the presence of significant magnetic anisotropy in these systems.

In order to investigate the dynamics of magnetization, ac magnetic susceptibility measurements were performed for all four compounds. No ac signals were observed for either of the Ho analogues **3** and **4**. For $Fe^{III}_4Er^{III}_2$ compound **1**, very weak out-of-phase ac signals were shown in zero dc field. However, under a dc field of 500 Oe, strong frequency-dependent in-phase and out-of-phase signals with well-defined peaks were detected (Fig. 4), indicating slow relaxation of magnetization and the suppression of quantum tunneling of magnetization (QTM) by applying a small external dc field. Fitting the data by an Arrhenius law results in an energy barrier U_{eff} = 12.8 K and relaxation time $\tau_0 = 4.6 \times 10^{-7}$ s (Fig. S3). By comparison, for the Fe_4Dy_2 analogue, clear peaks were shown in frequency-dependent out-of-phase plots under zero dc field, no quantum tunneling regime was observed, and U_{eff} and τ_0 were 21.4 K and 2.7×10^{-8} s, respectively.[35] The difference in the dynamics of magnetization for both compounds should not only result from the coordination environment of the Ln^{III} ions, but also from the interactions between the Ln^{III} ions and the paramagnetic Fe^{III} ions. Firstly, an approximately square antiprismatic configuration is preferable to maximize the anisotropy for the oblate Dy^{III} ions, rather than for the prolate Er^{III} ions.[25] Furthermore, weak 3d-4f interactions lead to the trigger of the QTM and diminishing the energy barrier, while strong 3d-4f exchange couplings suppress the QTM under zero dc field and slow down the relaxation of magnetization.[18-21]

The Cole-Cole plots for **1** under a 500 Oe dc field can be fitted based on a generalized Debye function (Fig. S4). The value of α parameter varies from 0.026 (at 2.5 K) to 0.25 (at 1.8 K), suggesting that the distribution of the relaxation time becomes larger on lowering the temperature. The large α value might result from the QTM at very low temperature.

Compound **2**, with diamagnetic Ga^{III} ions in place of the Fe^{III} ions in **1**, displayed temperature-dependent in-phase and out-of-phase ac signals under zero dc field, but no maxima were observed in the χ'' *vs. T* plots (Fig. 5), suggesting the presence of QTM or multi-relaxation processes in this system. However, by applying a small dc field of 750 Oe, clear maxima were detected in both χ'' *vs T* and χ'' *vs. v* plots (Fig. 6 and 7). Linear Arrhenius fitting of the frequency-dependent ac data gives an estimated energy barrier of U_{eff} = 53.5 K and the relaxation time $\tau_0 = 8.6 \times 10^{-9}$ s (Fig. S5). By replacing the paramagnetic Fe^{III} ions with the diamagnetic Ga^{III} ions, the energy barrier U_{eff}

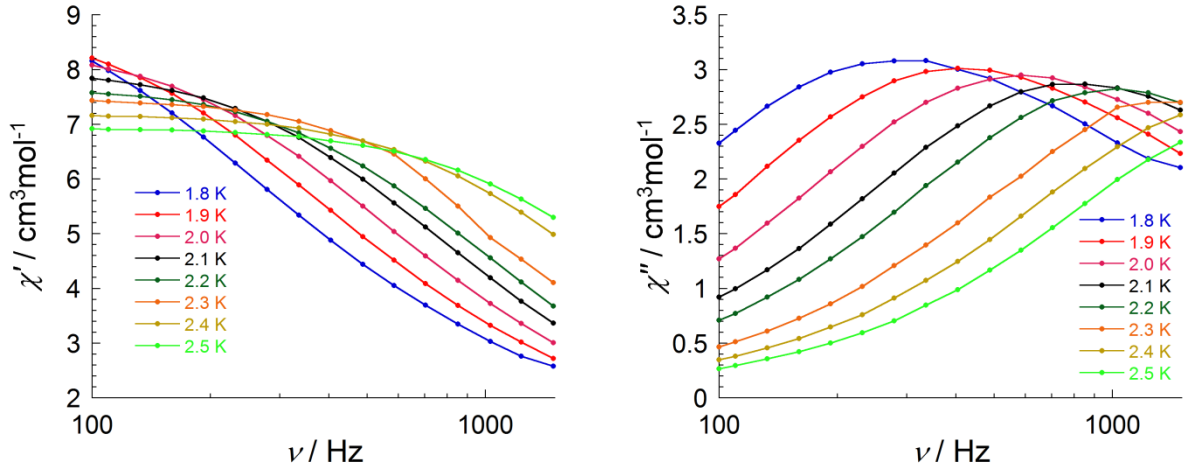

Fig. 4 Frequency dependence of the in-phase (χ') (top) and out-of-phase (χ'') (bottom) ac susceptibility components at different temperatures in a dc field of 500 Oe for **1**.

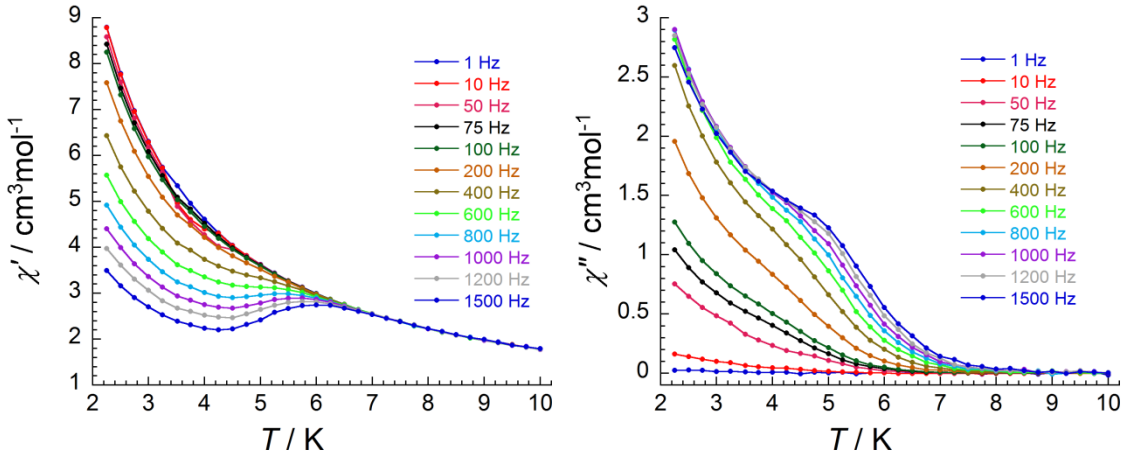

Fig. 5 Temperature dependence of the in-phase (χ') (left) and out-of-phase (χ'') (right) ac susceptibility components at different frequencies in zero dc field for **2**.

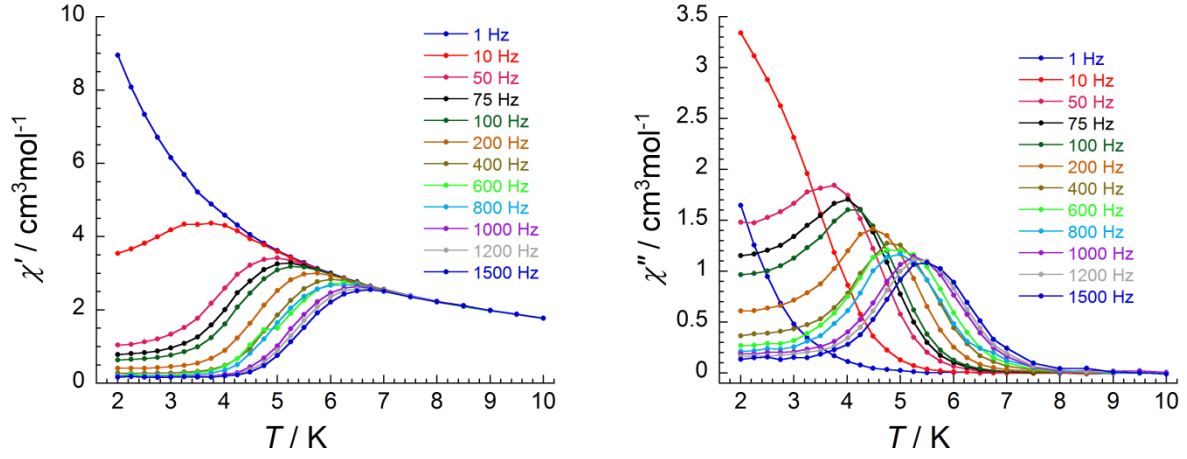

Fig. 6 Temperature dependence of the in-phase (χ') (left) and out-of-phase (χ'') (right) ac susceptibility components at different frequencies in a dc field of 750 Oe for **2**.

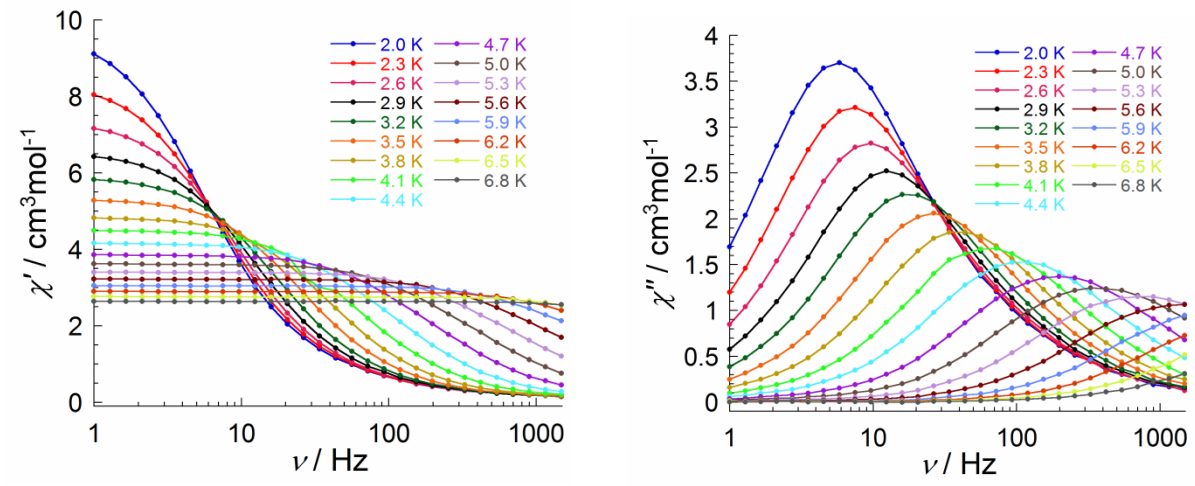

Fig. 7 Frequency dependence of the in-phase (χ') (left) and out-of-phase (χ'') (right) ac susceptibility components at different temperatures in a dc field of 750 Oe field for **2**.

increases from 12.8 K (for **1**) to 53.5 K (for **2**), confirming that the weak 3d-4f interaction enhances the QTM and reduces the energy barrier.[18,19] The Cole-Cole plots for **2** under 750 Oe dc field (Fig. S6) show symmetric semicircles and can be fitted to a generalized Debye function with α = 0.058 (at 6.2 K) - 0.22 (at 2.0 K). The relatively large α values within the low temperature regime indicate a wide distribution of relaxation time due to the incompletely quenched QTM.

Conclusions

We have reported the synthesis, structures and magnetic properties of four isostructural hexanuclear $M^{III}_4Ln^{III}_2$ coordination clusters, $[M_4Er_2(\mu_3\text{-}OH)_2(n\text{bdea})_4(C_6H_5COO)_8]\cdot$MeCN (M = Fe (**1**), Ga (**2**)) and $[M_4Ho_2(\mu_3\text{-}OH)_2(n\text{bdea})_4(C_6H_5COO)_8]\cdot$MeCN (M = Fe (**3**), Ga (**4**)). Upon systematic dc magnetic susceptibility studies on all four compounds and the recently reported isomorphous Fe_4Y_2 compound **5**, we found that the Er^{III}-Er^{III} interaction is ferromagnetic and the Fe^{III}-Er^{III} interactions are weak antiferromagnetic within Fe_4Er_2 compound **1**, while the Ho^{III}-Ho^{III} interaction is antiferromagnetic and the Fe^{III}-Ho^{III} interactions are negligible in Fe_4Ho_2 compound **3**. The ac magnetic susceptibility studies reveal that both Er^{III}-based compounds **1** and **2** exhibit SMM behavior. By replacing the Fe^{III} ions with diamagnetic Ga^{III} ions, the energy barrier increases from 12.8 K (for **1**) to 53.5 K (for **2**), indicating that the weak Fe^{III}-Er^{III} interactions enhance the QTM, leading to a lower energy barrier.

Acknowledgements

We acknowledge the Karlsruhe Institute of Technology for financial support.

Notes and references

1 G. Christou, D. Gatteschi, D. N. Hendrickson and R. Sessoli, *MRS Bull.*, 2000, **25**, 66.
2 D. N. Woodruff, R. E. P. Winpenny and R. A. Layfield, *Chem. Rev.*, 2013, **113**, 5110.
3 F. Habib and M. Murugesu, *Chem. Soc. Rev.*, 2013, **42**, 3278.
4 P. Zhang, Y.-N. Guo and J. Tang, *Coord. Chem. Rev.*, 2013, **257**, 1728.
5 R. Sessoli, A. K. Powell, *Coord. Chem. Rev.*, 2009, **253**, 2328.
6 M. Andruh, J.-P. Costes, C. Diaz and S. Gao, *Inorg. Chem.*, 2009, **48**, 3342.
7 G. E. Kostakis, I. J. Hewitt, A. M. Ako, V. Mereacre and A. K. Powell, *Phil. Trans. R. Soc. A*, 2010, **368**, 1509.
8 J. W. Sharples and D. Collison, *Coord. Chem. Rev.*, 2014, **260**, 1.
9 K. Liu, W. Shi and P. Cheng, *Coord. Chem. Rev.*, 2015, **289**, 74.
10 E. M. Pineda, N. F. Chilton, R. Marx, M. Dörfel, D. O. Sells, P. Neugebauer, S.-D. Jiang, D. Collison, J. van Slageren, E. J. L. McInnes and R. E. P. Winpenny, *Nat. Commun.*, 2014, **5**, 5243.
11 J. Long, F. Habib, P.-H. Lin, I. Korobkov, G. Enright, L. Ungur, W. Wernsdorfer, L. F. Chibotaru and M. Murugesu, *J. Am. Chem. Soc.*, 2011, **133**, 5319.
12 Y.-N. Guo, G.-F. Xu, W. Wernsdorfer, L. Ungur, Y. Guo, J. Tang, H.-J. Zhang, L. F. Chibotaru and A. K. Powell, *J. Am. Chem. Soc.*, 2011, **133**, 11948.
13 S. Schmidt, D. Prodius, G. Novitchi, V. Mereacre, G. E. Kostakis and A. K. Powell, *Chem. Commun.*, 2012, **48**, 9825.
14 S. Das, A. Dey, S. Kundu, S. Biswas, R. S. Narayanan, S. Titos-Padilla, G. Lorusso, M. Evangelisti, E. Colacio and V. Chandrasekhar, *Chem. Eur. J.*, 2015, **21**, 16955.
15 S. K. Langley, N. F. Chilton, L. Ungur, B. Moubaraki, L. F. Chibotaru and K. S. Murray, *Inorg. Chem.*, 2012, **51**, 11873.
16 S. K. Langley, L. Ungur, N. F. Chilton, B. Moubaraki, L. F. Chibotaru and K. S. Murray, *Inorg. Chem.*, 2014, **53**, 4303.
17 H. Xiang, W.-G. Lu, L. Jiang, W.-X. Zhang and Y. Lan, *Chem. Eur. J.*, 2016, **6**, 907.
18 E. M. Pineda, N. F. Chilton, F. Tuna, R. E. P. Winpenny and E. J. L. McInnes, *Inorg. Chem.*, 2015, **54**, 5930.
19 A. Bhunia, M. T. Gamer, L. Ungur, L. F. Chibotaru, A. K. Powell, Y. Lan, P. W. Roesky, F. Menges, C. Riehn and G. Niedner-Schatteburg, *Inorg. Chem.*, 2012, **51**, 9589.
20 S. K. Langley, D. P. Wielechowski, V. Vieru, N. F. Chilton, B. Moubaraki, B. F. Abrahams, L. F. Chibotaru and K. S. Murray, *Angew. Chem. Int. Ed.*, 2013, **52**, 12014.
21 S. K. Langley, D. P. Wielechowski, V. Vieru, N. F. Chilton, B. Moubaraki, L. F. Chibotaru and K. S. Murray, *Chem. Sci.*, 2014, **5**, 3246.
22 A. Okazawa, T. Shimada, N. Kojima, S. Yoshii, H. Nojiri and T. Ishida, *Inorg. Chem.*, 2013, **52**, 13351.
23 M. Sakamoto, K. Manseki and H. Okawa, *Coord. Chem. Rev.*, 2001, **219**, 379.

24 R. E. P. Winpenny, *Chem. Soc. Rev.*, 1998, **27**, 447.
25 J. D. Rinehart and J. R. Long, *Chem. Sci.*, 2011, **2**, 2078.
26 T. Han, Y.-S. Ding, J.-D. Leng, Z. Zheng and Y.-Z. Zheng, *Inorg. Chem.*, 2015, **54**, 4588.
27 Y.-S. Ding, T. Han, Y.-Q. Hu, M. Xu, S. Yang and Y.-Z. Zheng, *Inorg. Chem. Front.*, 2016, **3**, 798.
28 K.-X. Yu, Y.-S. Ding, T. Han, J.-D. Leng and Y.-Z. Zheng, *Inorg. Chem. Front.*, 2016, **3**, 1028.
29 Y.-S. Ding, N. F. Chilton, R. E. P. Winpenny and Y.-Z. Zheng, *Angew. Chem. Int. Ed.*, 2016, **55**, 16071.
30 L. Qin, Y.-Z. Yu, P.-Q. Liao, W. Xue, Z. Zheng, X.-M. Chen and Y.-Z. Zheng, *Adv. Mater.*, 2016, **28**, 10772.
31 T. Han, Y.-S. Ding and Y.-Z. Zheng, *Structure and Bonding*, Springer, 2016, 209.
32 G.-J. Zhou, Y.-S. Ding and Y.-Z. Zheng, *Dalton Trans.*, 2017, **46**, 3100.
33 A. Yamashita, A. Watanabe, S. Akine, T. Nabeshima, M. Nakano, T. Yamamura and T. Kajiwara, *Angew. Chem.*, 2011, **123**, 4102.
34 E. Lucaccini, L. Sorace, M. Perfetti, J.-P. Costes and R, Sessoli, *Chem. Commun.*, 2014, **50**, 1648.
35 S. Chen, V. Mereacre, C. E. Anson and A. K. Powell, *Dalton Trans.*, 2016, **45**, 98.
36 S. Chen, V. Mereacre, C. E. Anson and A. K. Powell, *Dalton Trans.*, 2016, **45**, 9336.
37 R. F. Weinland and A. Herz, *Berichte der Deutschen Chemischen Gesellschaft*, 1912, **45**, 266.
38 A. Baniodeh, *Cooperative Effects in Non-cyclic and cyclic FeIII/4f Coordination Clusters*, Ph.D. Thesis, Karlsruhe Institute of Technology (KIT), 2013, Cuvillier Verlag, ISBN 978-3-95404-448-1.
39 G. M. Sheldrick, *Acta Cryst*., 2015, **A71**, 3-8.
40 G. M. Sheldrick, *Acta Cryst*., 2015, **C71**, 3-8.